Cyclin-G-associated kinase GAK/dAux regulates autophagy initiation via ULK1/Atg1 in glia

Shiping Zhang[1†], Shuanglong Yi[1,5,†], Linfang Wang[1,5,†], Shuhua Li[1], Honglei Wang[1], Li Song[2], Jiayao Ou[2], Min Zhang[1], Ruiqi Wang[1], Mengxiao Wang[1], Yuchen Zheng[1], Kai Yang[3], Tong Liu[4], Margaret S. Ho[1,*]

[1]School of Life Science and Technology, ShanghaiTech University, Shanghai, 201210, China

[2]Department of Anatomy and Neurobiology, Tongji University School of Medicine, Shanghai, 200092, China

[3]International Academic Center of Complex Systems, Advanced Institute of Natural Sciences, Beijing Normal University at Zhuhai, 519087, China

[4]Institute of Neuroscience, State Key Laboratory of Neuroscience, CAS Center for Excellence in Brain Science and Intelligence Technology, Chinese Academy of Sciences, Shanghai, 200031, China

[5]University of Chinese Academy of Sciences, Beijing, 100049, China

[†]These authors contributed equally

[*]Corresponding author: Margaret S. Ho, Ph.D. Email: margareth@shanghaitech.edu.cn

Abstract

Autophagy is a major means for the elimination of protein inclusions in neurons in neurodegenerative diseases such as Parkinson's disease (PD). Yet, the mechanism of autophagy in the other brain cell type, glia, is less well characterized and remains largely unknown. Here we present evidence that the PD risk factor Cyclin G-associated kinase (GAK)/dAuxilin (dAux) is a new component in glial autophagy. GAK/dAux directly interacts with ULK1/Atg1 via its uncoating domain. Lack of GAK/dAux increases the autophagosome number and size in adult fly glia and mouse microglia, and generally upregulates levels of components in the initiation and PI3K class III complexes including ULK1/Atg1, demonstrating that GAK/dAux regulates the onset of glial autophagy. Consistently, lack of GAK/dAux enhances Atg1 and Atg9 trafficking to autophagosomes, promoting autophagy initiation. On the other hand, lack of GAK/dAux impairs the autophagic flux and blocks substrate degradation, suggesting that GAK/dAux might play additional roles in glial autophagy. Our findings identify a new autophagy factor in glia; considering the pivotal role of glia under pathological conditions, targeting glial autophagy is potentially a therapeutic strategy for PD.

Keywords: Autophagy; Glia; GAK; dAux; Parkinson's disease

Introduction

As the primary catabolic mechanism, macroautophagy (henceforth referred to as autophagy) was initially characterized as a bulk and non-selective degradation pathway induced by nutrient deprivation (1-3). Constitutive autophagy at the basal level, however, contributes to intracellular homeostasis in non-starved cells by degrading cellular materials like damaged organelles or misfolded proteins (4, 5). Interestingly, suppression of basal autophagy in the mouse nervous system results in the accumulation of ubiquitinated proteins and neurodegeneration (6, 7), whereas enhancing basal autophagy in the *Drosophila* nervous system promotes longevity and oxidant resistance (8). Furthermore, disease-associated mutations in core autophagy genes have been identified, supporting the link between autophagy and PD (9, 10). These findings mainly focus on a role for autophagy in neurons, as perturbation of such process leads to catastrophic consequences including pathological protein aggregation, deleterious lesions, and cell death (11). Whether autophagy in glia, the other major brain cell type, is executed via similar interplay using the same components as in neurons or other tissues, and whether it drives or contributes to disease pathology, remain largely unclear.

Studies from yeast and mammals provided fundamental insights into *de novo* autophagosome biogenesis mediated by the evolutionarily conserved autophagy-related (ATG) genes (4, 5, 12). Upon autophagy initiation, stress induces the recruitment of ATG1/UNC-51 like autophagy activating kinase 1 (ULK1) complex to the phagophore assembly site or the pre-autophagosomal structure (PAS). The ATG1/ULK1 complex

facilitates the assembly of phosphatidylinositol 3-kinase (PI3KC3) class III complex for PI3P production and promote the nucleation of the isolated membranes (also termed phagophores) (13). Whereas phagophore expansion is achieved by two ubiquitin-like conjugation steps: the formation of ATG12-ATG5 conjugate and ATG8 lipidation, additional lipids and proteins contributing to membrane expansion are delivered by the ATG9-containing vesicles derived from the Golgi apparatus, recycling endosomes or the plasma membrane (14-18). The expanded phagophores are sealed into a double-layered autophagosome, which eventually fuses with lysosome to form autolysosome, the milieu for degrading autophagic cargoes by acidic hydrolases.

Here we present evidence that the PD risk factor Cyclin G-associated kinase (GAK)/dAuxilin (dAux) is a new component in glial autophagy. GAK/dAux interacts with ULK1/Atg1 via the J domain with uncoating activity. GAK/dAux regulates the protein levels of ULK1/Atg1 and other components in the initiation and PI3K complexes controlling autophagy initiation. *In-vivo*, Lack of GAK/dAux increases the autophagosome number and size, and regulates the trafficking of ULK1/Atg1 and Atg9 to the autophagosomes. On the other hand, lack of GAK/dAux impairs autophagic flux and substrate degradation. Taken together, our findings identify a key factor regulating glial autophagy via controlling the activity of the initiation regulator ULK1/Atg1.

Results

Lack of dAux selectively increases the number of autophagosomes in adult fly glia

Identified in a behavior screen, the *Drosophila* homolog of the PD risk factor GAK, dAux, has been implicated in a broad spectrum of parkinsonian symptoms (19). GAK/dAux is a serine/threonine kinase that regulates clathrin-uncoating, cell cycle progression, and hepatitis C entry (20-23). Whereas another closely-related homolog for *GAK* (*DNAJC26*), *AUXILIN* (*DNAJC6*), is dominantly expressed in neurons, there is only one *Drosophila* homolog *dauxilin* (*daux*) that exhibits a higher homology with GAK (GAK 41.66%, AUXILIN 34.52%). GAK and dAux are both ubiquitiously expressed and shares a conserved kinase domain. To investigate dAux function at the cellular level, an RNAi line targeting *Drosophila daux* (*daux*-RNAi, V16182) was expressed to reduce *daux* expression in neurons or glia by the driver *GMR57C10-Gal4* or *repo-Gal4*, respectively. qRT-PCR, western blot (WB), and immunostaining analyses indicated that *daux* expression was efficiently reduced by the RNAi (Figures S1A-S1D).

Under these conditions, the morphology, distribution, and number of the autophagic organelles labeled by the marker mCherry.Atg8a were analyzed in different adult brain regions, including the region "Glia" enriched of glial processes, glial nuclei, and neuronal nuclei, and the region "Antenna Lobe, AL" enriched of axon neuropils in close proximity to glial processes (Figures 1A and 1B). Interestingly, downregulating *daux* expression by *daux*-RNAi pan-neuronally did not cause severe change in the number or size of the Atg8a-positive puncta (Figures S1E and S1F). Instead, downregulating *daux* expression in glia caused a significant increase in the number of Atg8a-positive puncta (Figures 1C and 1D). These results, confirmed by one additional

105 *daux*-RNAi (*daux*-RNAi$^{\#2}$, BL39017), an endogenous protein trap *pmCh.Atg8a*, anti-
106 Atg8a antibodies, and Mosaic Analysis with a Repressible Cell Marker (MARCM)
107 clones of *daux* mutant carrying EMS point mutations *I670K*, *L8H*, or *G257E* (24)
108 (Figures S1G, S1H, and 1E-1J,), indicated an increase in glial autophagic structures in
109 the absence of dAux. Results from using a different control *UAS-luciferase*-RNAi (*luc*-
110 RNAi) were also consistent (Figures S1I and S1J). Ultrastructural analysis by
111 Transmission Electron Microscopy (TEM) also showed an increase in the number of
112 autophagosomes, which exhibits typical double-membrane structure with a
113 characteristic cleft in-between and contains non-degraded cytoplasm, upon *daux*-RNAi
114 expression in glia (pink asterisks, Figures 1K and 1L). Moreover, whereas the Rab7-
115 positive late endosomes appeared in clusters with puncta number unaffected (Figures
116 S1K and S1L), the formation of the Rab5-positive early endosomes remained largely
117 intact upon glial dAux depletion (Figure S1M). Notably, expression of the fly dAux or
118 human GAK in glia rescued the *daux*-RNAi-induced increase in the autophagosome
119 number (Figures 1O and 1P). Taken together, these results indicate that dAux regulates
120 glial autophagosome number and the function of GAK/dAux is conserved across
121 species.
122
123 **Lack of Gak increases the number and size of autophagosomes in mouse microglia**
124 In addition, the mouse immortalized microglial cell line (IMG) and the primary mouse
125 microglia were examined for the effect of lacking Gak on autophagic structures. The

126 IMG cells were stained positive for ionized calcium-binding adapter molecule 1 (Iba1)
127 or transmembrane protein 119 (TMEM119), confirming their microglial identity
128 (Figures S2A and S2B). Consistent with the previously reported expression in microglia
129 and astrocytes (25, 26), Gak was also detected in the IMG cells (Figures S2C-S2G) (27).
130 Treatment with either of the two siRNAs targeting *Gak* reduced its expression in IMG
131 as shown by qRT-PCR, WB, and immunostaining analyses (Figures S2C-S2G). *Gak*
132 mRNA and protein expression were also reduced down to 50% and 60%, respectively
133 in *Gak* conditional knockout (cKO) mouse microglia (Figures S2H-S2J). We failed to
134 collect *Gak* cKO primary microglia for WB analysis of Gak protein levels due to
135 inefficient growth.

136 In IMG cells, treatment of either siRNA increased autophagosome size labeled by
137 the microtubule-associated protein 1A/1B-light chain 3 (LC3) (Figures 1Q and 1R).
138 Both the intensity and size of LC3 in microglia, and the LC3-Iba1 colocalization
139 increased in *Gak* cKO microglia, suggesting increased autophagosome number in
140 microglia (Figures 1S and 1T). Interestingly, the size of autophagosome consistently
141 increases in the IMG, *Gak* cKO microglia, and fly *daux* mutant MARCM clones, but
142 not *daux*-RNAi brains, possibly owing to the incomplete knock down by RNAi (Figures
143 1D, 1J, 1R, and 1T). Taken together, these results suggest that Gak regulates
144 autophagosome biogenesis in mouse microglia.

145

146 **Lack of GAK/dAux promotes autophagy initiation**

147 Based on the increase in the autophagosome number, it is conceivable that lack of glial
148 dAux induces or blocks autophagy. Interestingly, Atg8a-II protein levels in adult fly
149 brains downregulating glial dAux expression increased, which further increased in the
150 presence of Bafilomycin A1 (BafA1), an inhibitor blocking lysosome acidification and
151 autophagosome-lysosome fusion (28, 29) (Figures 2A and 2B). These results indicate
152 that lack of glial dAux still triggers increase in the autophagosome number even when
153 blocking the fusion, reinforcing a role for dAux in autophagy initiation. Using the anti-
154 ULK1 antibodies that also recognize the *Drosophila* Atg1 proteins as validated by *atg1*-
155 RNAi (Figures S3A and S3B), an increase in the number of ULK1-positive puncta was
156 detected upon glial dAux depletion (Figures 2C and 2D). In addition, components of
157 the initiation complex including Atg13, Atg6, and Atg14 were all affected as the number
158 of mCherry.Atg13-, GFP.Atg6-, and GFP.Atg14-positive puncta increased upon glial
159 dAux depletion (Figures 2C-2F). Notably, omegasomes labeled by two independent
160 reporters: GFP.ZFYVE1 (12, 30) and EGFP.DFCP1 (31), exhibited significant increase
161 in number upon glial *daux*-RNAi expression, with the size of EGFP.DFCP1-positive
162 omegasomes became significantly larger as fused by multiple smaller rings (Figures 2G
163 and 2H). Taken together, these results demonstrate the increased formation of
164 autophagosome precursors in the absence of glial dAux.

165 To better understand the mechanism of dAux-mediated autophagy initiation, we
166 turned to a different system, HeLa cells, for further characterization. A knockdown
167 system was established using two independent siRNAs targeting *GAK* (siRNA$^{\#1}$ and

siRNA[#2]). Treatment of either siRNA reduced *GAK* expression in HeLa cells as shown by WB and immunostaining analyses (Figures S3C-S3F). Interestingly, ULK1, ATG13, and BECLIN1 protein levels significantly increased while ATG14 protein levels exhibited an increasing trend upon *GAK* siRNA treatment, suggesting a general upregulation in autophagy initiation (Figures 2I and 2J). In addition, the mTORC1-mediated phosphorylation on the ULK1 Serine 757 (pS757-ULK1) decreased, suggesting that the ULK1 activity is enhanced as mTORC1 inhibition is relieved (Figures 2I and 2J). In addition, a *GAK* KO cell line was created by silencing the *GAK* expression in HeLa cells using CRISPR-Cas9 (Figures S3G-S3J). Consistent to the observations in flies, lack of GAK causes an increase in LC3-II protein levels in both *GAK* siRNA-treated and KO cells (Figures 2K and 2L, S3K and S3L). LC3-II protein levels also further increased in the presence of BafA1 in *GAK* siRNA-treated cells, reinforcing a direct role of GAK in autophagy initiation (Figures 2K and 2L). Taken together, these results indicate that autophagy initiation is induced in the absence of GAK/dAux; GAK/dAux regulates the onset of glial autophagy.

GAK/dAux interacts with ULK1/Atg1 and regulates its protein levels

As shown in flies and HeLa cells, lack of GAK/dAux enhances ULK1/Atg1 activity and induces autophagy initiation. We next tested if ULK1/Atg1 acts downstream of GAK/dAux in regulating autophagy initiation. Co-immunoprecipitation (Co-IP) analysis using fly S2 cells expressing Flag-dAux and Myc-Atg1 revealed a direct

189 interaction between dAux and Atg1 when pulling down Myc-Atg1 with the anti-Myc
190 beads. Reverse pull down by Flag-tagged dAux also revealed similar interaction (Figure
191 3A). To determine which dAux domain is responsible for Atg1 interaction, different
192 dAux deletion variants were made and expressed in flies for testing their interaction
193 with Atg1. All variants expressed properly except the one lacking PTEN domain
194 ($dAux^{\Delta PTEN}$, Figures 3B and 3C). Co-IP analysis showed that Atg1 interacts with most
195 of the dAux variants except the one lacking J domain ($dAux^{\Delta J}$, Figure 3D). In addition,
196 overexpression of $dAux^{\Delta Kinase}$ or $dAux^{\Delta J}$ enhanced ULK1 levels (Figures 3E and 3F).
197 Importantly, the early-onset PD SNP mutation in the J domain of AUXILIN (DNAJC6)
198 (32, 33) is conserved in dAux, and overexpressing the dAux carrying this mutation
199 $dAux^{DNAJC6m}$ enhanced ULK1 levels (Figures 3E and 3F). These results implicate that
200 dAux kinase and uncoating function are important for regulating the ULK1/Atg1
201 protein level.

202 On the other hand, GAK interacted with ULK1 in HEK293FT cells, but failed to
203 interact with ULK1 lacking the C-terminal domain ($ULK1^{\Delta CTD}$), suggesting that CTD
204 is required for GAK-ULK1 interaction (Figures 3G and 3H). Consistent to the enhanced
205 ULK1 activity, the ULK1 protein level was also elevated in *GAK* siRNA-treated HeLa
206 cells (Figures 3I-3L). To further test the relationship between dAux and Atg1, epistatic
207 genetic analysis between dAux and Atg1 was conducted. Silencing *atg1* expression in
208 glia caused a dramatic decrease in the number of omegasomes and autophagosomes,
209 reinforcing the master regulatory role of Atg1 in autophagy initiation (Figures 3M-3P).

Co-expression of *atg1*-RNAi and *daux*-RNAi rescued and further suppressed the *daux*-RNAi-induced increase in the number of omegasome and autophagosome, suggesting that dAux acts upstream of Atg1 in regulating autophagy initiation (Figures 3M-3P). Taken together, these results demonstrate that GAK/dAux interacts with ULK1/Atg1 and regulates its protein level.

dAux regulates Atg1 independently of its kinase function

Given that both dAux kinase and J domains are implicated in the Atg1 activation, phosphoproteomic analysis was subsequently conducted using adult fly head samples collected from control and *repo>daux*-RNAi flies (Figure S4A). These results revealed significant differences on the phosphorylation profiles of autophagy-related proteins (Figure S4B). Nonetheless, no significant changes were detected for Atg1 phosphorylation when downregulating dAux expression in glia. Only minor alternations on the two Atg1 residues, S282 (RNAi/LacZ ratio 1.131) and T292 (RNAi/LacZ ratio 1.053), were identified (Table S2). In addition, our Co-IP analysis revealed that $dAux^{\Delta Kinase}$ interacts with Atg1, indicating that the kinase domain is not essential for the interaction (Figure 3D). Despite that $dAux^{\Delta Kinase}$ expression enhances ULK1 levels, its impact on autophagy remains similar to dAux when analyzing the protein levels of Atg8a-II, Ubi, and P62 (Figures S4C-S4F), suggesting that lacking kinase domain does not hinder dAux function in autophagy. Hence, it is unlikely that dAux regulates Atg1 in a kinase-dependent manner.

Lack of GAK/dAux promotes ULK1/Atg1 trafficking to autophagosomes

One of the major steps in initiating autophagy is the ULK1/Atg1 transport to the autophagy initiation sites for forming the autophagosomes. We next analyzed the colocalization of ULK1/Atg1 with LC3/Atg8a as an indicator for the ULK1/Atg1 trafficking efficiency. Since an increase in the ULK1/Atg1 protein levels was also detected, we carefully chose the Manders' Correlation method when analyzing the colocalization given that the change in protein level is also considered in this statistical approach (34-36). Consistent to the observations in flies and mice, the number of LC3-positive puncta labeled by the transfected RFP-LC3 increased in the *GAK* siRNA-treated or KO cells (Figures 4A and 4B, S5A and S5B). In addition, the ULK1/Atg1 trafficking to the autophagosomes was enhanced as shown by the increased colocalization of ULK1/Atg1 and LC3/Atg8a in flies expressing *daux*-RNAi, *GAK* siRNA-treated, and KO HeLa cells (Figures 4A-4D, S5A and S5B). In contrast, the colocalization of ULK1 with TGN38-marked trans-Golgi network (TGN) decreased, further suggesting that ULK1 trafficking to the autophagosomes is enhanced when lacking GAK (Figures 4E and 4F, S5C and S5D). In support of these findings, ULK1 trafficking to the omegasomes also increased as the colocalization of ULK1 with transfected GFP-DFCP1 increased in the *GAK* siRNA-treated (Figures S5E and S5F) and KO cells (Figures S5G and S5H). Taken together, these results indicate that GAK/dAux regulates autophagy initiation via ULK1/Atg1 trafficking.

Glial dAux regulates Atg9 trafficking to autophagosomes via Atg1

In addition to promote Atg1 trafficking, lack of dAux increased the glial Atg9-Atg8a colocalization analyzed by the *mCherry.Atg8a* and *EGFP.Atg9* reporters, indicating that dAux also regulates Atg9 trafficking to autophagosomes (Figures 5A, 5A', and 5C). Next, live-cell imaging analysis was conducted, and the dynamic of Atg9 trafficking was analyzed by Imaris (Figures 5E-H, Supplementary Video 1 and 2). Interestingly, the speed of both Atg8a- and Atg9-positive puncta decreased upon glial dAux depletion, suggesting that these puncta are less mobile (Figures 5E and 5H). Notably, the duration of the Atg9-Atg8a contact was significantly longer, and the percentage of Atg9-positive puncta being trafficked to the vicinity of Atg8a-positive puncta (with a radius of 0.35 μm) was also significantly greater (Figures 5F and 5G). These results demonstrate that glial dAux regulates the dynamic of Atg9 trafficking to and its fall off from autophagosomes.

Consistent to the notion that Atg1 regulates Atg9 phosphorylation and transport (37-39), lacking Atg1 abolished Atg9 trafficking to the autophagosomes as the Atg9-Atg8a colocalization decreased significantly (Figures 5A, 5A', and 5C). These results suggest that dAux and Atg1 regulates Atg9 trafficking in opposite means. Interestingly, co-expression of *atg1*-RNAi and *daux*-RNAi rescued and further suppressed the dAux-mediated Atg9 trafficking (Figures 5B, 5B', and 5D), suggesting that dAux regulates Atg9 trafficking via Atg1. Given that Atg9 is a downstream target of Atg1, it is likely

273 that dAux-mediated Atg1 activation promotes Atg9 trafficking to the autophagosomes,
274 hence initiating autophagy.
275
276 **Lack of GAK/dAux impairs autophagic flux and substrate degradation**
277 To further demonstrate a role for dAux in glial autophagy, the autophagic flux was
278 analyzed using a dual reporter *UAS-GFP-mCherry-Atg8a* in *Drosophila* adult brains.
279 Whereas mCherry-positive puncta were GFP-negative and autophagy proceeded
280 normally in the control animals, autophagic flux was impaired in the absence of glial
281 dAux as both the GFP- and mCh-positive puncta colocalization and the intensity of
282 GFP puncta increased significantly upon glial dAux depletion. In the presence of BafA1,
283 the GFP- and mCh-positive puncta colocalization further increased upon depleting glial
284 dAux and a similar trend of GFP puncta intensity was detected (Figures 6A and 6B).
285 As these non-quenched GFP signals could represent either the non-fused
286 autophgasomes or the fused but dysfunctional autolysosomes, we next checked whether
287 the fusion of autophagosomes and lysosomes is affected by glial dAux depletion.
288 Interestingly, analysis of Lamp1-Atg8a colocalization with Stimulated Emission
289 Depletion (STED) imaging on adult fly brains expressing *daux*-RNAi revealed an
290 increased number of enlarged and well-colocalized autolysosomes, indicating that
291 lysosomes are able to fuse with autophagosomes (Figures 6C and 6D). Ultrastructural
292 TEM analysis also showed an increase in the number of autolysosomes, which have
293 only one limiting membrane and contain electron dense cytoplasmic materials and/or

organelles, upon *daux*-RNAi expression in glia (blue arrows, Figures 1K and 1N). Reducing the expression of fusion factors such as *syx17* or *vamp7* caused a block in fusion (40), and co-expression of either RNAi reverted the *daux*-RNAi-induced increase in Lamp1-Atg8a colocalization (Figures S6A and S6B). These results suggest that some successful fusion occurs so that increasing number of enlarged autolysosomes is detected.

As a consequence, inhibiting dAux expression in glia caused the accumulation of autophagic substrates such as Ref(2)P (the *Drosophila* ortholog of P62) and Ubiquitin (Ubi) (Figures 6E-6H). P62 and Ubi were also accumulated in *Gak* siRNA-treated IMG cells (Figures 6I and 6J), *GAK* siRNA-treated and *GAK* KO HeLa cells (Figures 6K, 6L, S3K, and S3L). Furthermore, increased Ref(2) puncta observed upon *daux*-RNAi expression in glia were well localized with autophagosomes and lysosomes (Figure S6C), suggesting that theses fused autolysosomes are able to recognize and encircle protein substrates, but failed to degrade them. Taken together, these findings suggest that GAK/dAux regulates glial autophagy via the initiation step but with an ultimate effect on impaired flux and substrate degradation (Figure 6M).

Discussion

Our findings pinpoint a role for GAK/dAux in autophagy initiation. Despite that the ultimate consequence for lacking GAK/dAux blocks autophagic substrate degradation and a potential compensatory mechanism leading to the increased autophagosome

biogenesis might exist, our evidence indicates that GAK/dAux functions directly on autophagy initiation by modulating ULK1/Atg1 activity and protein level. First, the dAux-mediated increase in the Atg8a-II/I protein levels is further enhanced by the presence of BafA1, indicating that autophagy is promoted even when substrate degradation is blocked. Lack of GAK/dAux also causes an increase in phagophore nucleation and omegasome formation, suggesting that these earlier steps in autophagy initiation are all affected. Furthermore, the levels of components in the initiation and PI3K class III complexes including ULK1/Atg1, ATG13, BECLIN1, and ATG14 all increase in the absence of GAK, indicating a general upregulation in autophagy initiation. It has been shown that mTOR senses the nutrient-rich condition and blocks autophagic induction by phosphorylating ULK1 at S757 to prevent its activation (41). In the absence of GAK, S757 phosphorylation is significantly decreased, indicating enhanced ULK1 activity. Thus, GAK/dAux suppresses autophagy initiation; it is conceivable that GAK/dAux acts as a glial sensor to control the onset of autophagy for sensing pathological signals like protein inclusions.

ULK1/Atg1 is a master regulator initiating autophagy. In complex with ATG13 and FIP200, ULK1/Atg1 initiates autophagy by phosphorylating a vast array of downstream components including the factors in the initiation and PI3P class III complexes (42-44). The ULK1/Atg1 activity undergoes intricate controls by post-translational modification including phosphorylation, acetylation, or ubiquitination (45, 46). These modifications can either activate or inhibit ULK1/Atg1 activity, thereby

promoting or inhibiting autophagy, respectively. Despite that a direct interaction between GAK/dAux and ULK1/Atg1 is detected, our phosphoproteomic analysis reveals no significant alternation on Atg1 phosphorylation upon glial dAux depletion. In addition, dAux lacking the kinase activity remains associated with Atg1. Thus, it is unlikely that GAK/dAux regulates ULK1/Atg1 via phosphorylation.

Previous studies reported that inhibiting ULK1 kinase activity, either by ULK1 inhibitors or expressing a kinase-dead ULK1, caused accumulation of stalled early autophagosomal structures (47, 48). While we observe some phenotypes similar to stalled early autophagosomes, but with crucial differences. First, instead of lacking LC3-II flux, we observed increased LC3-II flux with/without BafA1 when downregulating GAK/dAux both in HeLa cells and fly. Immunostaining of dual autophagy flux reporter in adult fly brains with BafA1 got similar results. Second, the accumulated autophagosomes were able to fuse with lysosomes to form autolysosomes when downregulating glial dAux. Third, we observed substantial co-localization of autophagosomes, lysosomes, and Ref(2)P, suggesting that theses fused autolysosomes are able to recognize and encircle protein substrates, but failed to degrade them. Last but most importantly, we observed decreased S757 phosphorylation in the absence of GAK, indicating enhanced ULK1 activity.

As we demonstrated that dAux J domain is required for its interaction with Atg1, it is conceivable that dAux regulates Atg1 via its uncoating function. Expression of dAux lacking the J domain or dAux carrying a conserved early-onset PD SNP mutation

in the J domain causes an increase in the ULK1 protein level. These results implicate the relevance of dAux clathrin-uncoating activity with ULK1/Atg1. In addition, it is also possible that GAK/dAux contributes to the recycling of ULK1/Atg1 from autophagosomes to TGN, thus leading to similar enhancement on autophagy initiation. To this end, our live-cell imaging analysis supports the notion that dAux plays dual roles in the context of Atg9 trafficking to autophagosomes. As increased amount of Atg9-positive puncta is detected at the vicinity of Atg8a-positive puncta, the contact duration time between Atg9 and Atg8a is also significantly enhanced in the absence of dAux. Thus, dAux might be needed for both the anterograde trafficking to and the recycling from autophagosomes. On the other hand, our results support a competition model for how GAK initiates autophagy. GAK interacts with the C-terminus of ULK1, the domain also required for its interaction with Atg13 (49). It is reasonable to spectulate that GAK competes with Atg13 for ULK1 binding. In the absence of GAK, increased amounts of ULK1 proteins are relieved from the inhibition for interaction with Atg13 and together trafficked to the omegasomes/autophagosomes for autophagy initiation.

Despite an effect on autophagy initiation, autophagic flux and substrate degradation were impaired in the absence of glial dAux. Recently, two independent studies reported the involvement of GAK in autophagy and lysosomal homeostasis. Munson et. al. reported that GAK inhibition alters lysosomal morphology in U2OS cells (50). After treatment of GAK kinase inhibitor, increased lysosome numbers and large

autolysosome structures were observed, possibly mediated by the increased TFEB nuclear localization (50). Miyazaki et. al. found that *GAK* KO or GAK kinase inhibitor treatment could induce autophagosome accumulation and enlarged autolysosomes in A549 cells, which were caused by impaired autophagosome-lysosome fusion and autophagic lysosome reformation (ALR) (51). Given that we demonstrated that the fusion can still occur, it is possible that lysosome function is affected so that flux and substrate degradation are impaired upon glial dAux depletion. Consistent to this notion, the number and size of glial Lamp1-positive lysosomes were increased in adult fly brains expressing the *daux*-RNAi (Figures S6D and S6E). Ultrastructural TEM analysis also showed an increase in the number and size of lysosome, which exhibits smaller and electron dense structures with single-membrane, upon *daux*-RNAi expression in glia (yellow and red arrows, Figures 1K and 1M). Thus, it is feasible that GAK/dAux regulates autophagy at multiple steps via different mechanisms.

In the present study, we identify a new autophagy factor in glia and elucidate its regulatory mechanism on autophagy initiation. Our findings provide new insights on glial autophagy and advance the understanding of PD pathology from a glial perspective. Future work will be required to investigate how GAK/dAux plays different roles in glia and neurons, and how it contributes to neurodegeneration in a tissue-specific manner.

Materials and Methods

All animal experiments were conducted according to proper regulation and guideline under ShanghaiTech. Details of fly and mouse genotypes are included in SI Appendix and Table S1. Methods including cell lines and transfections, molecular cloning, immunohistochemistry, *in-vivo* time lapse analysis, TEM, phosphoproteomic analysis, biochemistry, confocal microscopy, and statistical analysis are described in the SI Appendix.

Acknowledgments

We thank Bloomington *Drosophila* Stock Center, Vienna *Drosophila* RNAi Center, Tsinghua Fly Center, the Core Facility of *Drosophila* Resource and Technology, Shanghai Institute of Biochemistry and Cell Biology, Chinese Academy of Sciences, Developmental Studies Hybridoma Bank, Chao Tong, Henry C. Chang, Lei Xue, Henry Sun, Tor Erik Rusten, Gabor Juhasz, Patrik Verstreken, Aike Guo, Yijun Liu, and Gerald M Rubin for fly stocks and antibodies; Chih-Hao Lee for IMG cell line; Yanfeng Liu for HeLa and HEK293FT cell lines; Kangmin He for HeLa *GAK* KO cell line; Jiawei Zhou for *CX3CR1-Cre* mice. We also thank the Molecular Imaging Core Facility (MICF), the Molecular and Cell Biology Core Facility (MCBCF), and the Multi-Omics Core Facility (MOCF) at the School of Life Science and Technology, ShanghaiTech University for providing technical support; Yu Kong and Lijun Pan in Electron Microscopy Facilities of Center for Excellence in Brain Science and Technology, Chinese Academy of Science for assistance with TEM sample preparation; Wei-Chung

Lee for help on TEM; Ho lab members for discussion and comments. This work was supported by grants from ShanghaiTech and National Natural Science Foundation of China (31871039 and 32170962).

Author contributions

S.Z, S.Y, L.W, and M.S.H conceived and designed the study. S.Z, S.Y, L.W, S.L, H.W, L.S, J.O, M.Z, R.W, M.W, Y.Z, K.Y, T.L, and M.S.H performed the experiments. S.Z, S.Y, L.W, S.L, and M.S.H analyzed the data. M.S.H wrote the paper with the input of S.Z, S.Y, and L.W. All authors read and approved the manuscript.

Declaration of Interests

The authors declare no competing interests.

Figure Legends

Figure 1. Lack of Gak/dAux increases the number and size of autophagosome in glia

(**A** and **B**) Illustration (A) and representative images (B) of an adult fly brain showing the expression pattern of glial cells. *repo-GAL4* drives the expression of *UAS-IVS-Syn21-GFP-p10* (*repo>IVS-Syn21-GFP-p10*) that labels both membrane and nucleus of glia. Dashed squares in yellow and blue indicate the relative positions of “Glia” and the antenna lobe (“AL”) assessed throughout the study. The regions “Glia” are enriched

441 with GFP-positive glial membrane (green), GFP- and Repo-positive glial nuclei (green
442 and magenta), as well as Elav-positive neuronal nuclei (red). The regions "AL" are
443 enriched with axon neuropils and glial processes (green). (**C** and **D**) Representative
444 images (C) and quantifications (D) of autophagosomes in the Whole brain, "Glia", and
445 "AL". Glial autophagosomes (red) were labeled with *repo-GAL4* driven *UAS-*
446 *mCherry.Atg8a* (*UAS-mCherry.Atg8a; repo-GAL4*). Note that downregulating glial
447 *daux* induced an increase in the autophagosome number in both "Glia" and "AL". (**E-**
448 **H**) Representative images (E and G) and quantifications (F and H) of the "Glia" region
449 in adult fly brains carrying an endogenous mCherry protein trap at the promoter of
450 *Atg8a* (*pmCh.Atg8a*, E) or stained with the anti-Atg8a antibodies (G). Note that similar
451 to *UAS-mCh.Atg8a*, the autophagosome number and fluorescent intensities in "Glia"
452 region increased upon expressing the *daux*-RNAi in glia. (**I** and **J**) Glial MARCM
453 clones of *daux* mutants ($daux^{L78H}$, $daux^{G257E}$, and $daux^{I670K}$) expressing the *UAS-*
454 *mCh.Atg8a* by *repo-GAL4,* and adult fly brain "Glia" region were shown. Dashed lines
455 encircle the clonal area. Note that the number and size of glial autophagosomes per
456 clone increased in $daux^{G257E}$ and $daux^{I670K}$ mutants. (**K-N**) Representative TEM images
457 (K) and quantifications of autophagosome (L), lysosome (M), and autolysosome (N) in
458 "Glia" region of control and *repo>daux*-RNAi adult fly brains. Note an increase in the
459 number of autophagosome (pink asterisks), lysosome (yellow arrows) with the presence
460 of large lysosome-like structure (red arrows), and autolysosome (blue arrows) when
461 *daux*-RNAi was expressed in glia. (**O** and **P**) Co-expression of fly dAux or human GAK

(hGAK) rescued the *daux*-RNAi-induced increase in glial autophagosome number in "Glia" region. (**Q** and **R**) Representative images (Q) and quantifications (R) of LC3-positive autophagosomes in IMG cells treated with either *Gak* siRNA. Note that LC3-positive autophagosomes were enlarged upon abolishing *Gak* expression. (**S** and **T**) Representative images (S) and quantifications (T) of LC3-positive autophagosome in mouse SN microglia deficient of *Gak* at 36 weeks. In addition to the increase in the intensity and size of LC3 in Iba1^{+} microglia, the colocalization of Iba1 with LC3 also increased upon microglial Gak depletion. Scale bars and the sample number n are indicated in the Figures. For each experiment, more than three biologically independent replicates were done. Whereas results were consistent, representative results from one experiment was shown. A serial confocal Z-stack sections were taken with 0.4 μm each, and representative single layer images acquired at the similar plane of brains across all genotypes are shown, except mouse brain slices (S) shown as maximal projection. For TEM, more than 40 images from at least 5 independent adult fly brains of each genotype were analyzed. Colocalization is analyzed using the Pearson's Correlation and present as the Pearson's R value. Quantification figures from the same images but with different parameters are shown under the same label unless noted otherwise. Data are shown as mean ± SEM. P-values of significance (indicated with asterisks, ns no significance, * $p<0.05$, ** $p<0.01$, and *** $p<0.001$) are calculated by two-tailed unpaired t-test, Mann-Whitney test, ordinary one-way ANOVA followed by Tukey's multiple

482 comparisons test, or Kruskal-Wallis tests followed by Dunn's multiple comparisons test.

483 All genotypes analyzed are listed in Table S1.

484

485 **Figure 2. Lack of GAK/dAux promotes autophagy initiation**

486 (**A** and **B**) Representative WB images (A) and quantifications (B) of Atg8a-II protein

487 levels in the control and *repo>daux*-RNAi adult fly brains. Note that lack of glial dAux

488 increased Atg8a-II protein levels, and BafA1 treatment further increased the Atg8a-II

489 levels. (**C**-**H**) Representative images (C, E, G) and quantifications (D, F, H) of ULK1-,

490 mCh.Atg13-, GFP.Atg6-, GFP.Atg14-, GFP.ZFYVE1-, and EGFP.DFCP1-positive

491 puncta in "Glia" region of control and *repo>daux*-RNAi adult fly brains. *Drosophila*

492 Atg1 was detected using the mammal anti-ULK1 antibodies. Note that lack of glial

493 dAux increased the puncta number of all above, indicating a general upregulation in

494 autophagy initiation, phagophore nucleation, and omegasome formation. (**I**-**L**)

495 Representative WB images (I, K) and quantifications (J, L) of different autophagy

496 protein levels in *GAK* siRNA-treated HeLa cells. Results from two independent siRNAs,

497 *GAK* siRNA$^{\#1}$ and *GAK* siRNA$^{\#2}$, were consistent. Note that *GAK* knockdown

498 significantly increased the protein levels of pS757-ULK1, ATG13, BECN1, and LC3-

499 II. LC3-II protein level enhanced by *GAK* knockdown was further enhanced in the

500 presence of BafA1. Scale bars and the sample number n are indicated in the Figures.

501 For each experiment, more than three biologically independent replicates were done.

502 Whereas results were consistent, representative results from one experiment was shown.

503 A serial confocal Z-stack sections were taken with 0.4 μm each, and representative
504 single layer images acquired at the similar plane of brains across all genotypes are
505 shown. Colocalization is analyzed using the Pearson's Correlation and present as the
506 Pearson's R value. Data are shown as mean ± SEM. P-values of significance (indicated
507 with asterisks, ns no significance, * $p<0.05$, ** $p<0.01$, and *** $p<0.001$) are calculated
508 by two-tailed unpaired t-test, Mann-Whitney test, or ordinary one-way ANOVA
509 followed by Tukey's multiple comparisons test.

510

511 **Figure 3. GAK/dAux interacts with ULK1/Atg1 and regulates its protein levels**

512 (**A**) Co-IP analysis using fly S2 cells expressing Flag-dAux, Myc-Atg1, or both
513 revealed a direct interaction between dAux and Atg1. dAux or Atg1 was detected in the
514 pull down of Myc-Atg1 or Flag-dAux, respectively. (**B** and **C**) dAux variants lacking
515 different domains or carrying an early-onset PD SNP mutation (DNAJC6m) were
516 constructed and expressed in fly, adult heads were used for WB to check the expression
517 level. Note that $dAux^{\Delta PTEN}$ expressed poorly. (**D**) Different dAux variants were
518 expressed in S2 cells, and analyzed for their interaction with Atg1. Note that J domain
519 was required for dAux-Atg1 interaction. (**E** and **F**) Representative images (E) and
520 quantifications (F) of the ULK1 puncta number in the "Glia" region of adult fly brains
521 expressing different dAux variants. Note that the ULK1 puncta number increased when
522 expressing $dAux^{\Delta Kinase}$, $dAux^{\Delta J}$, or $dAux^{DNAJC6m}$. (**G** and **H**) N-terminal EGFP-fused
523 ULK1 variants lacking different domains were constructed, expressed in HEK293FT

524 cells, and analyzed for their interaction with GAK. Note that ULK1 lacking the C-
525 terminal domain CTD failed to interact with GAK. (**I-L**) The representative
526 immunostaining (I) and WB (K) images and quantifications (J and L) of the ULK1
527 protein level in *GAK* siRNA-treated HeLa cells. Note that *GAK* knockdown caused an
528 increase in the number and size of the ULK1 puncta, also the ULK1 protein level. (**M-**
529 **P**) Epistatic genetic analysis revealed that dAux acts upstream of Atg1 in regulating
530 autophagy initiation. Co-expression of *atg1*-RNAi in glia rescueed and further
531 suppressed the *daux*-RNAi-induced increase in the number of GFP.ZFYVE1- and
532 mCh.Atg8a-positive puncta in "Glia" region. Scale bars and the sample number n are
533 indicated in the Figures. For each experiment, more than three biologically independent
534 replicates were done. Whereas results were consistent, representative results from one
535 experiment was shown. A serial confocal Z-stack sections were taken with 0.4 μm each,
536 and representative single layer images acquired at the similar plane are shown. Data
537 are shown as mean ± SEM. P-values of significance (indicated with asterisks, ns no
538 significance, * $p<0.05$, ** $p<0.01$, and *** $p<0.001$) are calculated by Mann-Whitney
539 test, ordinary one-way ANOVA followed by Tukey's multiple comparisons test, or
540 Kruskal-Wallis tests followed by Dunn's multiple comparisons test.
541
542 **Figure 4. GAK/dAux regulates ULK1/Atg1 trafficking from TGN to**
543 **autophagosomes**
544 (**A** and **B**) HeLa cells transfected with RFP-LC3 in the presence or absence of the *GAK*

siRNA were collected for immunostaining analysis with the anti-ULK1 antibodies. Note that both the LC3-positive puncta number and the ULK1 (green)-LC3 (red) colocalization increased upon GAK depletion. (**C** and **D**) ULK1-Atg8a colocalization was analyzed in "Glia" region of adult fly brains expressing mCh.Atg8a (*repo>mCh.Atg8a*) to label glial autophagosomes. Note that ULK1 (green)-Atg8a (red) colocalization increased in the absence of glial dAux. (**E** and **F**) ULK1 (green)-TGN38 (red) colocalization is analyzed in *GAK* siRNA-treated HeLa cells. Note that ULK1-TGN38 colocalization decreased, suggesting enhanced ULK1 trafficking to the autophagosomes upon GAK depletion. Areas enclosed by the white dashed squares in the representative images (A, C, and E) are enlarged in A', C', and E'. HeLa cell nuclei were stained with DAPI (blue). Scale bars and the sample number n are indicated in the Figures. For each experiment, more than three biologically independent replicates were done. Whereas results were consistent, representative results from one experiment was shown. A serial confocal Z-stack sections were taken with 0.4 μm each, and representative single layer images acquired at the similar plane are shown. Colocalization is analyzed using the Manders' Correlation, taking into account the change in the protein level. Data are shown as mean ± SEM. P-values of significance (indicated with asterisks, ns no significance, * $p<0.05$, ** $p<0.01$, and *** $p<0.001$) are calculated by two-tailed unpaired t-test or ordinary one-way ANOVA followed by Tukey's multiple comparisons test.

Figure 5. dAux-mediated Atg9 trafficking depend on Atg1

(**A**-**D**) Atg9 trafficking is investigated by analyzing the Atg9 (green)-Atg8a (red) colocalization in the "Glia" region of adult fly brains expressing the *UAS-EGFP.Atg9* and *UAS-mCh.Atg8a* reporters (*UAS-mCh.Atg8a; repo-GAL4, UAS-EGFP.Atg9*). Note that *daux*-RNAi or *atg1*-RNAi expression in glia caused a significant increase or decrease in the Atg9-Atg8a colocalization, respectively. Co-expression of *daux*-RNAi and *atg1*-RNAi rescued and further suppressed the increased Atg9-Atg8a colocalization. Areas enclosed by the white dashed squares in the representative images (A and B) are enlarged in A' and B'. (**E**-**H**) Live-cell imaging (E) and quantifications (F-H) of Atg9 trafficking to Atg8a in "Glia" region of adult fly brains. Note the percentage of Atg9-positic puncta being trafficked to the vicinity of Atg8a-positive puncta (with a radius of 0.35 um) was increased (F), the duration of the Atg9-Atg8a contacting was longer (G), and the speed of both Atg8a- and Atg9-positive puncta were decreased upon glial dAux depletion (H). Scale bars and the sample number n are indicated in the Figures. For each experiment, more than three biologically independent replicates were done. Whereas results were consistent, representative results from one experiment was shown. A serial confocal Z-stack sections were taken with 0.4 μm each, and representative single layer images acquired at the similar plane are shown. Colocalization is analyzed using the Manders' Correlation, taking into account the change in the protein level. Data are shown as mean ± SEM. P-values of significance (indicated with asterisks, ns no significance, * $p<0.05$, ** $p<0.01$, and *** $p<0.001$) are calculated by two-tailed

unpaired t-test, Mann-Whitney test, ordinary one-way ANOVA followed by Tukey's multiple comparisons test, or Kruskal-Wallis tests followed by Dunn's multiple comparisons test.

Figure 6. Lack of GAK/dAux impairs autophagic flux and substrate degradation

(**A** and **B**) Autophagic flux was impaired as examined by expressing the flux reporter *UASp-GFP-mCh-Atg8a*. Both the GFP- and mCh-positive puncta colocalization and the intensity of GFP puncta in "Glia" region increased upon depleting glial dAux. In the presence of BafA1, the GFP- and mCh-positive puncta colocalization further increased upon depleting glial dAux, a similar trend of GFP puncta intensity was detected but not statistically significant. Note that GFP- and mCh-positive puncta were enlarged and potentially dysfunctional due to the non-quenched GFP signals. (**C** and **D**) Representative confocal/STED images (C) and quantifications (D) of Lamp1- and Atg8a-positive puncta in "Glia" region of adult fly brains. Note that dAux depletion in glia increased the number and size of glial autolysosomes and the colocalization of autophagosomes and lysosomes. (**E**-**H**) Autophagic substrates such as Ref(2)P (the *Drosophila* P62 homolog) and Ubiquitin (Ubi) accumulated in *repo>daux*-RNAi adult fly brains as revealed by immunostaining ("Glia" region) and WB analyses. (**I** and **J**) P62 and Ubi protein levels increased upon *Gak* depletion in IMG cells. (**K** and **L**) P62 and Ubi protein levels increased upon *GAK* depletion in HeLa cells. (**M**) A model illustrating the regulating roles of GAK/dAux in glial autophagy. In *GAK/daux*-

deficient glia, lack of GAK/dAux activates ULK1/Atg1, upregulates protein levels of components in the initiation and PI3P class III complexes, and enhances Atg1 trafficking to the autophagosomes (thicker black arrows). dAux also regulates Atg9 trafficking to the autophagosomes via Atg1. These actions promote autophagy initiation and start the glial clearance program for substrates degradation. On the other hand, despite the benefits of inducing glial autophagy, lack of GAK/dAux also disrupts autophagic flux and substrate degradation. GAK/dAux regulatory steps are highlighted in green. Scale bars and the sample number n are indicated in the Figures. For each experiment, more than three biologically independent replicates were done. Whereas results were consistent, representative results from one experiment was shown. A serial confocal Z-stack sections were taken with 0.4 μm each, and representative single layer images acquired at the similar plane of brains across all genotypes are shown. Data are shown as mean ± SEM. P-values of significance (indicated with asterisks, ns no significance, * $p<0.05$, ** $p<0.01$, and *** $p<0.001$) are calculated by two-tailed t-test or ordinary one-way ANOVA followed by Tukey's multiple comparisons test.

References

1. Mizushima N (2018) A brief history of autophagy from cell biology to physiology and disease. *Nat Cell Biol* 20(5):521-527.
2. Dikic I & Elazar Z (2018) Mechanism and medical implications of mammalian autophagy. *Nat Rev Mol Cell Biol* 19(6):349-364.
3. Mizushima N & Komatsu M (2011) Autophagy: renovation of cells and tissues. *Cell* 147(4):728-741.
4. Mizushima N (2020) The ATG conjugation systems in autophagy. *Curr Opin Cell Biol* 63:1-10.

633 5. Galluzzi L, *et al.* (2017) Molecular definitions of autophagy and related
634 processes. *EMBO J* 36(13):1811-1836.
635 6. Hara T, *et al.* (2006) Suppression of basal autophagy in neural cells causes
636 neurodegenerative disease in mice. *Nature* 441(7095):885-889.
637 7. Komatsu M, *et al.* (2006) Loss of autophagy in the central nervous system
638 causes neurodegeneration in mice. *Nature* 441(7095):880-884.
639 8. Simonsen A, *et al.* (2008) Promoting basal levels of autophagy in the nervous
640 system enhances longevity and oxidant resistance in adult Drosophila.
641 *Autophagy* 4(2):176-184.
642 9. Deng Z, *et al.* (2017) Autophagy Receptors and Neurodegenerative Diseases.
643 *Trends Cell Biol* 27(7):491-504.
644 10. Levine B & Kroemer G (2019) Biological Functions of Autophagy Genes: A
645 Disease Perspective. *Cell* 176(1-2):11-42.
646 11. Kulkarni A, Chen J, & Maday S (2018) Neuronal autophagy and intercellular
647 regulation of homeostasis in the brain. *Curr Opin Neurobiol* 51:29-36.
648 12. Klionsky DJ, *et al.* (2016) Guidelines for the use and interpretation of assays
649 for monitoring autophagy (3rd edition). *Autophagy* 12(1):1-222.
650 13. Russell RC, *et al.* (2013) ULK1 induces autophagy by phosphorylating Beclin-
651 1 and activating VPS34 lipid kinase. *Nat Cell Biol* 15(7):741-750.
652 14. Mari M, *et al.* (2010) An Atg9-containing compartment that functions in the
653 early steps of autophagosome biogenesis. *J Cell Biol* 190(6):1005-1022.
654 15. Yamamoto H, *et al.* (2012) Atg9 vesicles are an important membrane source
655 during early steps of autophagosome formation. *J Cell Biol* 198(2):219-233.
656 16. Orsi A, *et al.* (2012) Dynamic and transient interactions of Atg9 with
657 autophagosomes, but not membrane integration, are required for autophagy.
658 *Mol Biol Cell* 23(10):1860-1873.
659 17. Puri C, Renna M, Bento CF, Moreau K, & Rubinsztein DC (2014) ATG16L1
660 meets ATG9 in recycling endosomes: additional roles for the plasma membrane
661 and endocytosis in autophagosome biogenesis. *Autophagy* 10(1):182-184.
662 18. Ravikumar B, Moreau K, Jahreiss L, Puri C, & Rubinsztein DC (2010) Plasma
663 membrane contributes to the formation of pre-autophagosomal structures. *Nat*
664 *Cell Biol* 12(8):747-757.
665 19. Song L, *et al.* (2017) Auxilin Underlies Progressive Locomotor Deficits and
666 Dopaminergic Neuron Loss in a Drosophila Model of Parkinson's Disease. *Cell*
667 *Rep* 18(5):1132-1143.
668 20. Zhang CX, *et al.* (2005) Multiple roles for cyclin G-associated kinase in
669 clathrin-mediated sorting events. *Traffic* 6(12):1103-1113.
670 21. Lee DW, Wu X, Eisenberg E, & Greene LE (2006) Recruitment dynamics of
671 GAK and auxilin to clathrin-coated pits during endocytosis. *J Cell Sci* 119(Pt
672 17):3502-3512.
673 22. He K, *et al.* (2020) Dynamics of Auxilin 1 and GAK in clathrin-mediated traffic.
674 *J Cell Biol* 219(3).

23. Shimizu H, Nagamori I, Yabuta N, & Nojima H (2009) GAK, a regulator of clathrin-mediated membrane traffic, also controls centrosome integrity and chromosome congression. *J Cell Sci* 122(Pt 17):3145-3152.
24. Zhou X, *et al.* (2011) Auxilin is required for formation of Golgi-derived clathrin-coated vesicles during Drosophila spermatogenesis. *Development* 138(6):1111-1120.
25. Zhang Y, *et al.* (2014) An RNA-sequencing transcriptome and splicing database of glia, neurons, and vascular cells of the cerebral cortex. *J Neurosci* 34(36):11929-11947.
26. Zhang Y, *et al.* (2016) Purification and Characterization of Progenitor and Mature Human Astrocytes Reveals Transcriptional and Functional Differences with Mouse. *Neuron* 89(1):37-53.
27. McCarthy RC, *et al.* (2016) Characterization of a novel adult murine immortalized microglial cell line and its activation by amyloid-beta. *J Neuroinflammation* 13:21.
28. Mauvezin C, Nagy P, Juhasz G, & Neufeld TP (2015) Autophagosome-lysosome fusion is independent of V-ATPase-mediated acidification. *Nat Commun* 6:7007.
29. Yoshimori T, Yamamoto A, Moriyama Y, Futai M, & Tashiro Y (1991) Bafilomycin A1, a specific inhibitor of vacuolar-type H(+)-ATPase, inhibits acidification and protein degradation in lysosomes of cultured cells. *J Biol Chem* 266(26):17707-17712.
30. Liu W, Duan X, Fang X, Shang W, & Tong C (2018) Mitochondrial protein import regulates cytosolic protein homeostasis and neuronal integrity. *Autophagy* 14(8):1293-1309.
31. Melani M, *et al.* (2017) Zonda is a novel early component of the autophagy pathway in Drosophila. *Mol Biol Cell* 28(22):3070-3081.
32. Elsayed LE, *et al.* (2016) A Novel Nonsense Mutation in DNAJC6 Expands the Phenotype of Autosomal-Recessive Juvenile-Onset Parkinson's Disease. *Ann Neurol* 79(2):335-337.
33. Olgiati S, *et al.* (2016) DNAJC6 Mutations Associated With Early-Onset Parkinson's Disease. *Ann Neurol* 79(2):244-256.
34. Bido S, *et al.* (2021) Microglia-specific overexpression of alpha-synuclein leads to severe dopaminergic neurodegeneration by phagocytic exhaustion and oxidative toxicity. *Nat Commun* 12(1):6237.
35. Nabar NR, *et al.* (2022) LRRK2 is required for CD38-mediated NAADP-Ca(2+) signaling and the downstream activation of TFEB (transcription factor EB) in immune cells. *Autophagy* 18(1):204-222.
36. Winslow AR, *et al.* (2010) alpha-Synuclein impairs macroautophagy: implications for Parkinson's disease. *J Cell Biol* 190(6):1023-1037.
37. Papinski D, *et al.* (2014) Early steps in autophagy depend on direct phosphorylation of Atg9 by the Atg1 kinase. *Mol Cell* 53(3):471-483.

38. Reggiori F, Tucker KA, Stromhaug PE, & Klionsky DJ (2004) The Atg1-Atg13 complex regulates Atg9 and Atg23 retrieval transport from the pre-autophagosomal structure. *Dev Cell* 6(1):79-90.
39. Zhou C*, et al.* (2017) Regulation of mATG9 trafficking by Src- and ULK1-mediated phosphorylation in basal and starvation-induced autophagy. *Cell Res* 27(2):184-201.
40. Hegedus K, Takats S, Kovacs AL, & Juhasz G (2013) Evolutionarily conserved role and physiological relevance of a STX17/Syx17 (syntaxin 17)-containing SNARE complex in autophagosome fusion with endosomes and lysosomes. *Autophagy* 9(10):1642-1646.
41. Kim J, Kundu M, Viollet B, & Guan KL (2011) AMPK and mTOR regulate autophagy through direct phosphorylation of Ulk1. *Nat Cell Biol* 13(2):132-141.
42. Karanasios E*, et al.* (2013) Dynamic association of the ULK1 complex with omegasomes during autophagy induction. *J Cell Sci* 126(Pt 22):5224-5238.
43. Papinski D & Kraft C (2016) Regulation of Autophagy By Signaling Through the Atg1/ULK1 Complex. *J Mol Biol* 428(9 Pt A):1725-1741.
44. Pengo N, Agrotis A, Prak K, Jones J, & Ketteler R (2017) A reversible phospho-switch mediated by ULK1 regulates the activity of autophagy protease ATG4B. *Nat Commun* 8(1):294.
45. Hurley JH & Young LN (2017) Mechanisms of Autophagy Initiation. *Annu Rev Biochem* 86:225-244.
46. Park JM*, et al.* (2016) The ULK1 complex mediates MTORC1 signaling to the autophagy initiation machinery via binding and phosphorylating ATG14. *Autophagy* 12(3):547-564.
47. Petherick KJ*, et al.* (2015) Pharmacological inhibition of ULK1 kinase blocks mammalian target of rapamycin (mTOR)-dependent autophagy. *J Biol Chem* 290(18):11376-11383.
48. Zachari M, Longo M, & Ganley IG (2020) Aberrant autophagosome formation occurs upon small molecule inhibition of ULK1 kinase activity. *Life Sci Alliance* 3(12).
49. Chan EY, Longatti A, McKnight NC, & Tooze SA (2009) Kinase-inactivated ULK proteins inhibit autophagy via their conserved C-terminal domains using an Atg13-independent mechanism. *Mol Cell Biol* 29(1):157-171.
50. Munson MJ*, et al.* (2021) GAK and PRKCD are positive regulators of PRKN-independent mitophagy. *Nat Commun* 12(1):6101.
51. Miyazaki M*, et al.* (2021) Targeted disruption of GAK stagnates autophagic flux by disturbing lysosomal dynamics. *Int J Mol Med* 48(4).

Figure 1

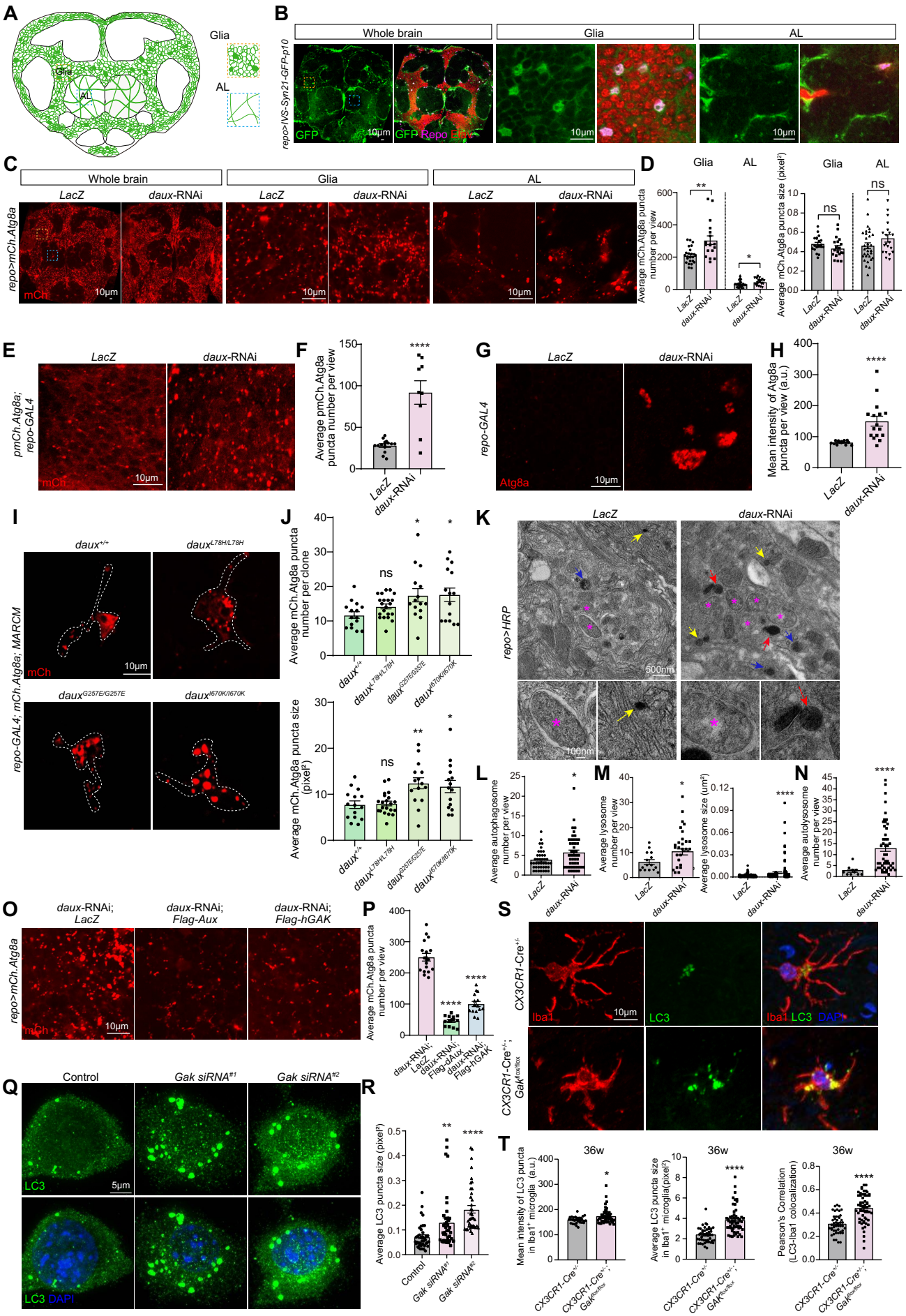
A
Glia
AL
B
Whole brain
Glia
AL
repo>IVS-Syn21-GFP-p10
GFP
GFP Repo
10μm
C
Whole brain
Glia
AL
LacZ
daux-RNAi
repo>mCh.Atg8a
mCh
10μm
D
Glia
AL
Average mCh.Atg8a puncta number per view
Average mCh.Atg8a puncta size (pixel²)
ns
E
LacZ
daux-RNAi
pmCh.Atg8a; repo-GAL4
mCh
10μm
F
Average pmCh.Atg8a puncta number per view
****
G
repo-GAL4
Atg8a
H
Mean intensity of Atg8a puncta per view (a.u.)
I
daux+/+
daux L78H/L78H
daux G257E/G257E
daux I670K/I670K
repo-GAL4; mCh.Atg8a; MARCM
J
Average mCh.Atg8a puncta number per clone
Average mCh.Atg8a puncta size (pixel²)
K
repo>HRP
500nm
100nm
L
Average autophagosome number per view
M
Average lysosome number per view
Average lysosome size (um²)
N
Average autolysosome number per view
O
daux-RNAi; LacZ
daux-RNAi; Flag-Aux
daux-RNAi; Flag-hGAK
P
Average mCh.Atg8a puncta number per view
S
CX3CR1-Cre+/-
CX3CR1-Cre+/-; Gakflox/flox
Iba1
LC3
DAPI
Q
Control
Gak siRNA#1
Gak siRNA#2
5μm
R
Average LC3 puncta size (pixel²)
T
36w
Mean intensity of LC3 puncta in Iba1+ microglia (a.u.)
Average LC3 puncta size in Iba1+ microglia(pixel²)
Pearson's Correlation (LC3-Iba1 colocalization)

Figure 2

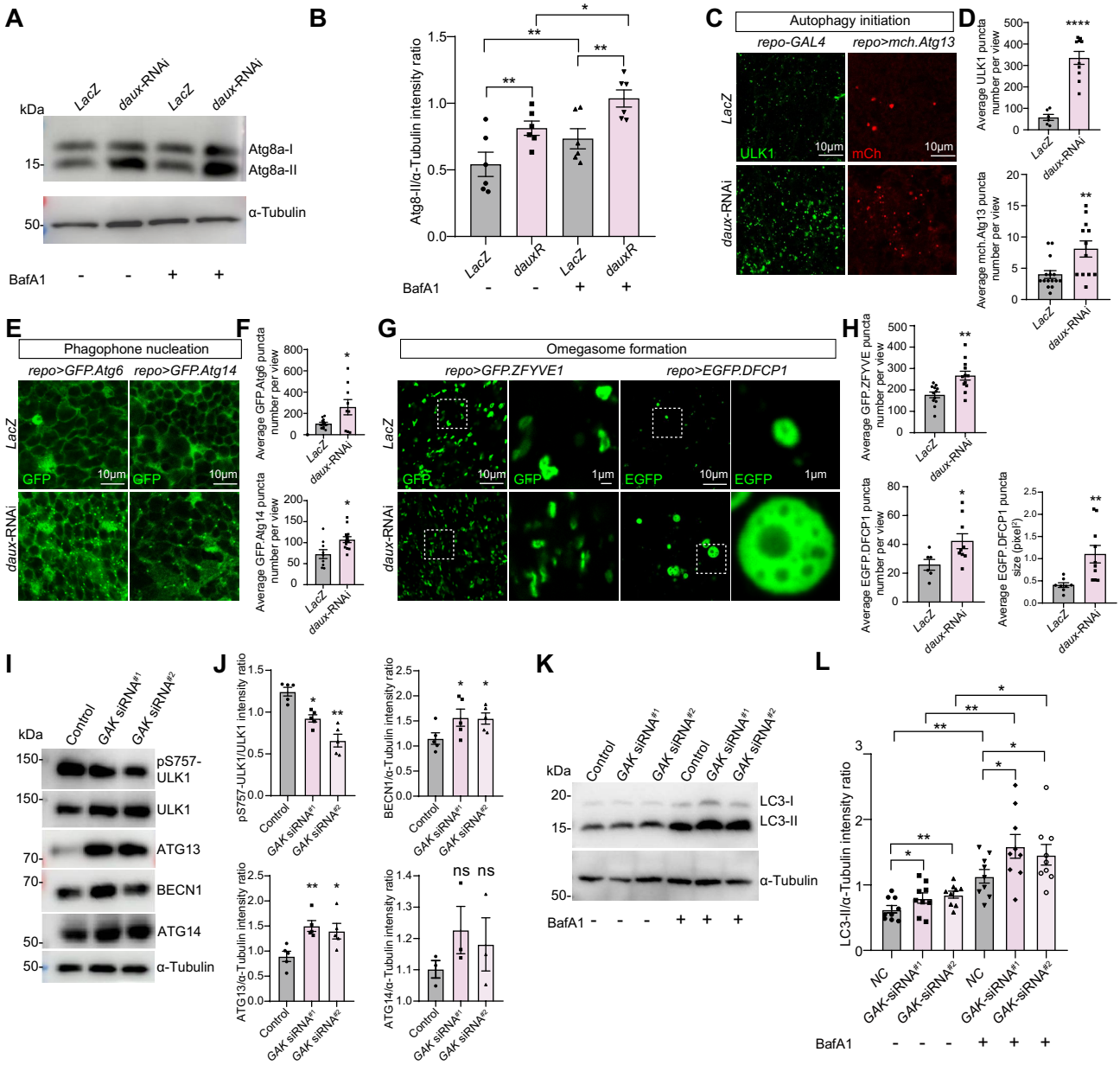
A
kDa
LacZ
daux-RNAi
LacZ
daux-RNAi
15-
Atg8a-I
Atg8a-II
50-
α-Tubulin
BafA1 - - + +
B
Atg8-II/α-Tubulin intensity ratio
LacZ
dauxR
LacZ
dauxR
BafA1 - - + +
C
Autophagy initiation
repo-GAL4
repo>mch.Atg13
LacZ
daux-RNAi
ULK1
mCh
10μm
D
Average ULK1 puncta number per view
Average mch.Atg13 puncta number per view
E
Phagophone nucleation
repo>GFP.Atg6
repo>GFP.Atg14
GFP
F
Average GFP.Atg6 puncta number per view
Average GFP.Atg14 puncta number per view
G
Omegasome formation
repo>GFP.ZFYVE1
repo>EGFP.DFCP1
EGFP
1μm
H
Average GFP.ZFYVE puncta number per view
Average EGFP.DFCP1 puncta number per view
Average EGFP.DFCP1 puncta size (pixel²)
I
Control
GAK siRNA#1
GAK siRNA#2
pS757-ULK1
ULK1
ATG13
BECN1
ATG14
α-Tubulin
J
pS757-ULK1/ULK1 intensity ratio
BECN1/α-Tubulin intensity ratio
ATG13/α-Tubulin intensity ratio
ATG14/α-Tubulin intensity ratio
ns
K
LC3-I
LC3-II
α-Tubulin
BafA1 - - - + + +
L
LC3-II/α-Tubulin intensity ratio
NC
GAK-siRNA#1
GAK-siRNA#2
BafA1 - - - + + +

Figure 3

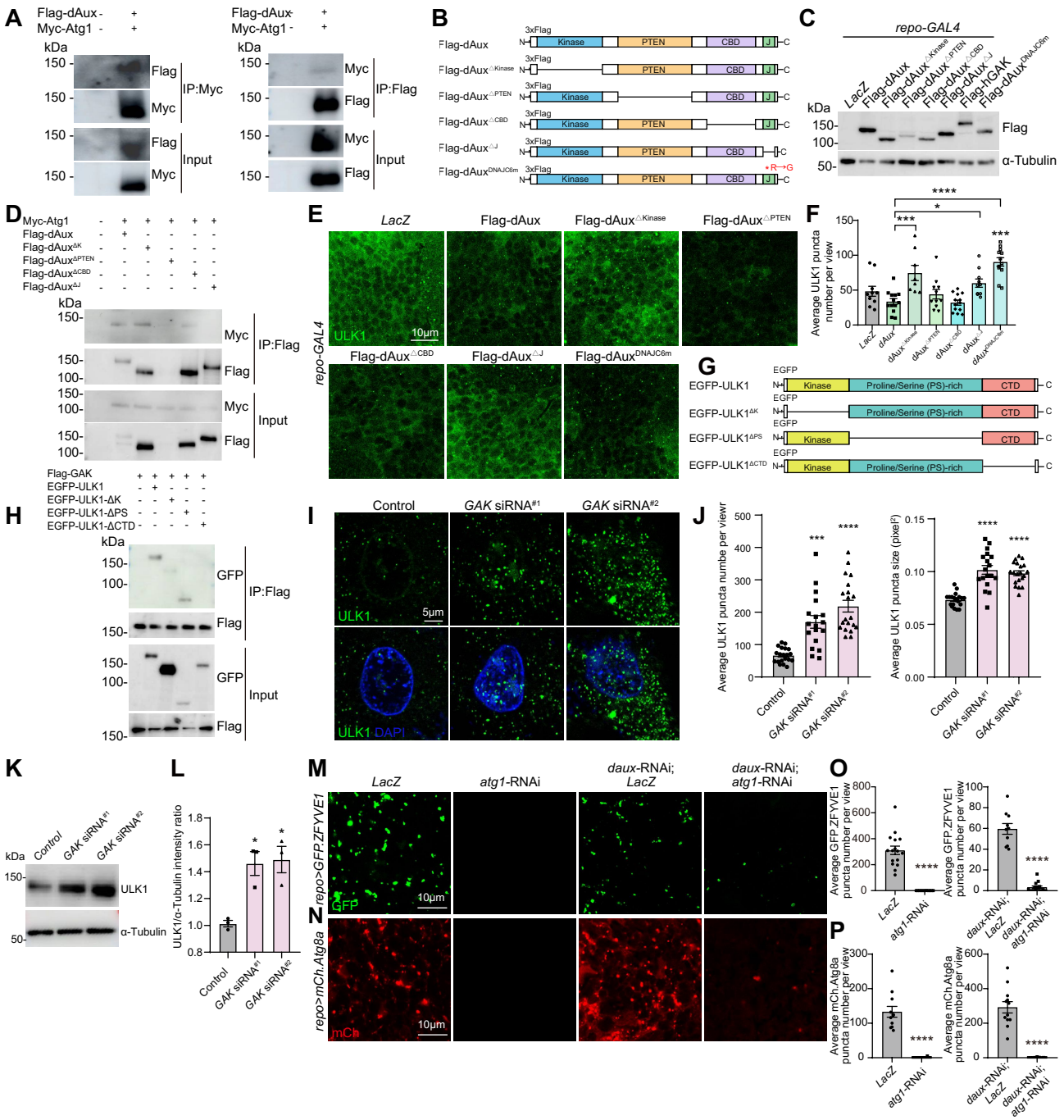
A
Flag-dAux
Myc-Atg1
kDa
150
Flag
Myc
IP:Myc
Input
IP:Flag
B
3xFlag
Flag-dAux
Flag-dAux△Kinase
Flag-dAux△PTEN
Flag-dAux△CBD
Flag-dAux△J
Flag-dAuxDNAJC6m
Kinase
PTEN
CBD
J
N
C
R→G
C
repo-GAL4
LacZ
Flag-dAux
Flag-dAux△Kinase
Flag-dAux△PTEN
Flag-dAux△CBD
Flag-dAux△J
Flag-hGAK
Flag-dAuxDNAJC6m
kDa
150
100
50
Flag
α-Tubulin
D
Myc-Atg1
Flag-dAux
Flag-dAuxΔK
Flag-dAuxΔPTEN
Flag-dAuxΔCBD
Flag-dAuxΔJ
Myc
Flag
IP:Flag
Input
Flag-GAK
EGFP-ULK1
EGFP-ULK1-ΔK
EGFP-ULK1-ΔPS
EGFP-ULK1-ΔCTD
GFP
E
LacZ
Flag-dAux
Flag-dAux△Kinase
Flag-dAux△PTEN
Flag-dAux△CBD
Flag-dAux△J
Flag-dAuxDNAJC6m
repo-GAL4
ULK1
10μm
F
Average ULK1 puncta number per view
150
100
50
0
***
*
****
G
EGFP
EGFP-ULK1
EGFP-ULK1ΔK
EGFP-ULK1ΔPS
EGFP-ULK1ΔCTD
Kinase
Proline/Serine (PS)-rich
CTD
H
I
Control
GAK siRNA#1
GAK siRNA#2
ULK1
5μm
ULK1 DAPI
J
Average ULK1 puncta numbe per viewr
500
400
300
200
100
0
Average ULK1 puncta size (pixel²)
0.15
0.10
0.05
0.00
Control
GAK siRNA#1
GAK siRNA#2
K
kDa
Control
GAK siRNA#1
GAK siRNA#2
150
50
ULK1
α-Tubulin
L
ULK1/α-Tubulin intensity ratio
1.8
1.6
1.4
1.2
1.0
0.8
M
LacZ
atg1-RNAi
daux-RNAi; LacZ
daux-RNAi; atg1-RNAi
repo>GFP.ZFYVE1
GFP
10μm
N
repo>mCh.Atg8a
mCh
O
Average GFP.ZFYVE1 puncta number per view
800
600
400
200
0
100
80
60
40
20
P
Average mCh.Atg8a puncta number per view
300
200
100
0
600
400
200
0

Figure 4

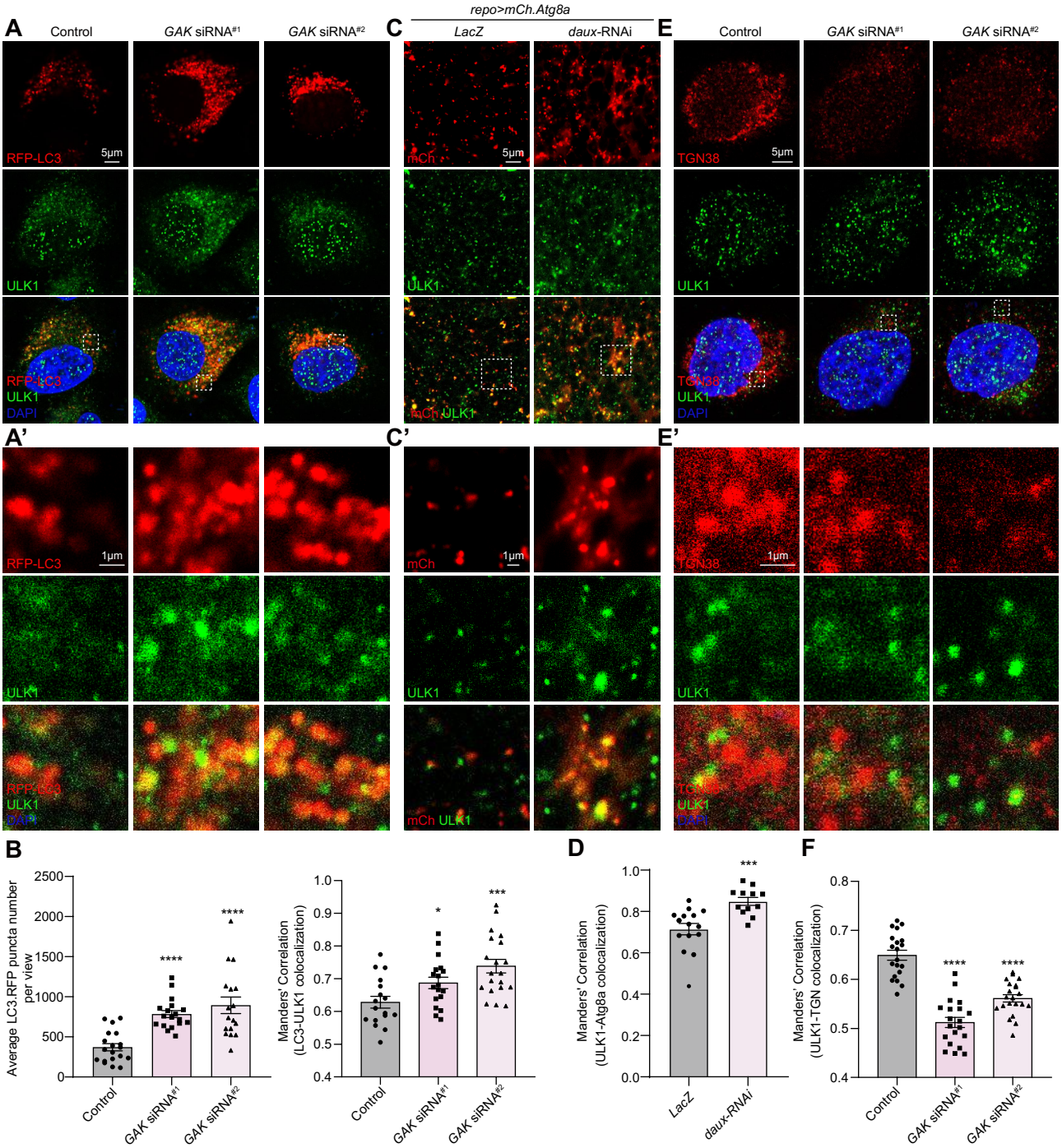
A
Control
GAK siRNA#1
GAK siRNA#2
C
repo>mCh.Atg8a
LacZ
daux-RNAi
E
Control
GAK siRNA#1
GAK siRNA#2
RFP-LC3
5μm
mCh
5μm
TGN38
5μm
ULK1
RFP-LC3
ULK1
DAPI
mCh ULK1
TGN38
ULK1
DAPI
A'
C'
E'
RFP-LC3
1μm
mCh
1μm
TGN38
1μm
ULK1
RFP-LC3
ULK1
DAPI
mCh ULK1
TGN38
ULK1
DAPI
B
Average LC3.RFP puncta number per view
2500
2000
1500
1000
500
0
****
****
Control
GAK siRNA#1
GAK siRNA#2
Manders' Correlation (LC3-ULK1 colocalization)
1.0
0.9
0.8
0.7
0.6
0.5
0.4
*
***
Control
GAK siRNA#1
GAK siRNA#2
D
Manders' Correlation (ULK1-Atg8a colocalization)
1.0
0.8
0.6
0.4
0.2
0.0
***
LacZ
daux-RNAi
F
Manders' Correlation (ULK1-TGN colocalization)
0.8
0.7
0.6
0.5
0.4
****
****
Control
GAK siRNA#1
GAK siRNA#2

Figure 5

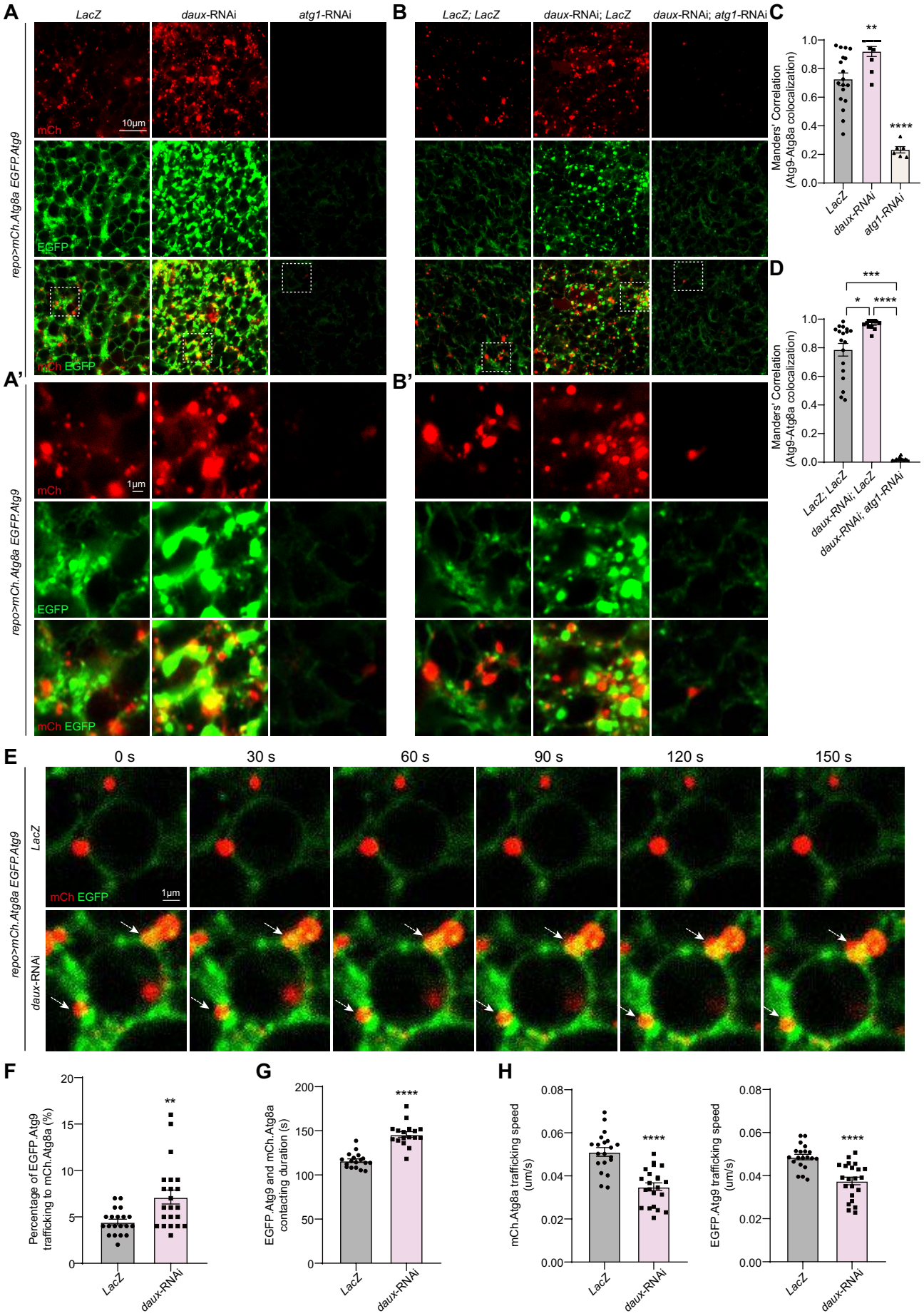
A
LacZ
daux-RNAi
atg1-RNAi
B
LacZ; LacZ
daux-RNAi; LacZ
daux-RNAi; atg1-RNAi
C
D
A'
B'
repo>mCh.Atg8a EGFP.Atg9
mCh
EGFP
mCh EGFP
10μm
1μm
Manders' Correlation (Atg9-Atg8a colocalization)
LacZ
daux-RNAi
atg1-RNAi
LacZ; LacZ
daux-RNAi; LacZ
daux-RNAi; atg1-RNAi
E
0 s
30 s
60 s
90 s
120 s
150 s
repo>mCh.Atg8a EGFP.Atg9
LacZ
daux-RNAi
F
Percentage of EGFP.Atg9 trafficking to mCh.Atg8a (%)
G
EGFP.Atg9 and mCh.Atg8a contacting duration (s)
H
mCh.Atg8a trafficking speed (um/s)
EGFP.Atg9 trafficking speed (um/s)

Figure 6

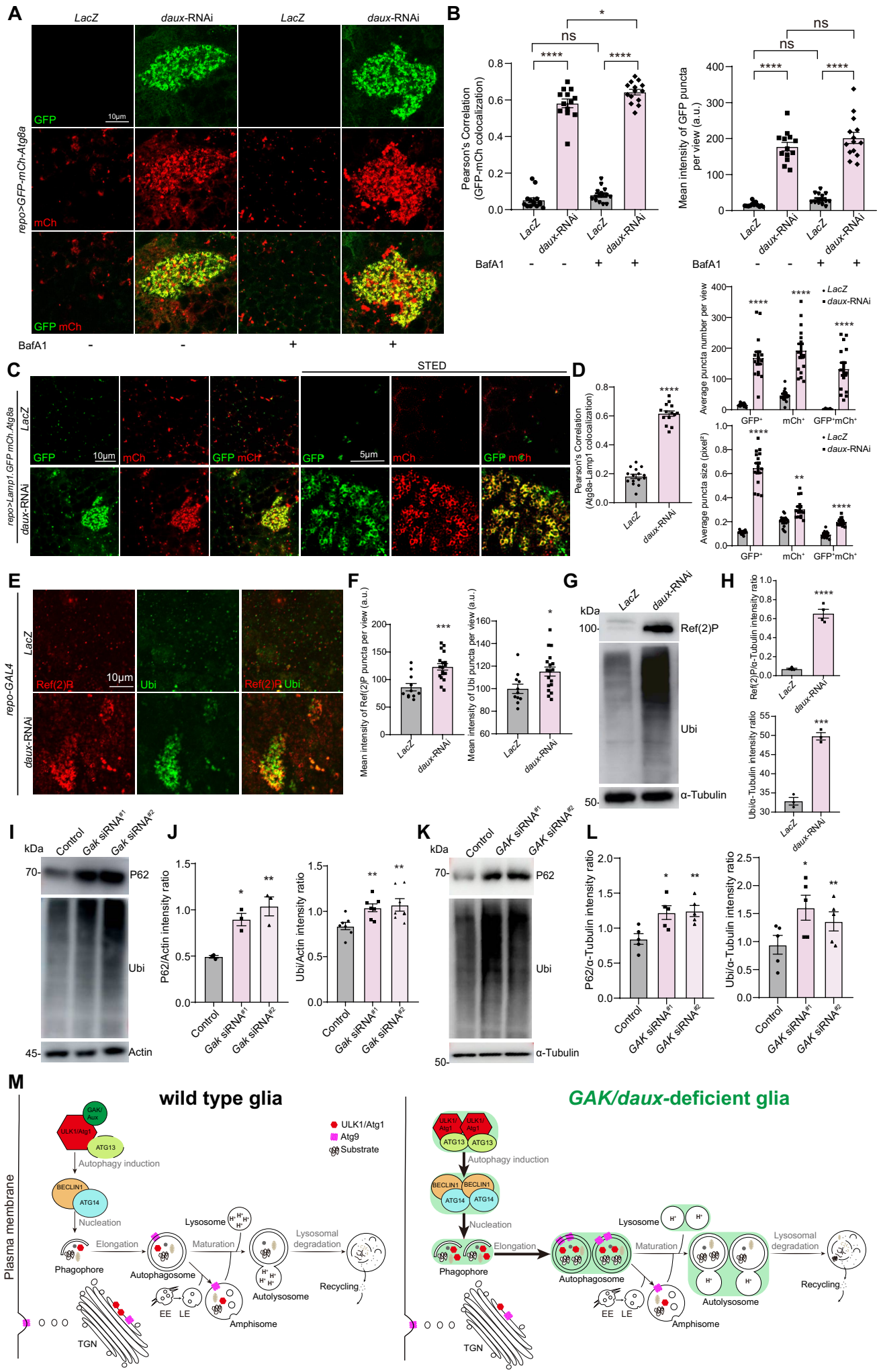
A
LacZ
daux-RNAi
repo>GFP-mCh-Atg8a
GFP
mCh
GFP mCh
10μm
BafA1
B
Pearson's Correlation (GFP-mCh colocalization)
Mean intensity of GFP puncta per view (a.u.)
ns
*
****
C
STED
repo>Lamp1.GFP mCh.Atg8a
5μm
D
Pearson's Correlation (Atg8a-Lamp1 colocalization)
Average puncta number per view
Average puncta size (pixel²)
GFP⁺
mCh⁺
GFP⁺mCh⁺
E
repo-GAL4
Ref(2)P
Ubi
Ref(2)P Ubi
F
Mean intensity of Ref(2)P puncta per view (a.u.)
Mean intensity of Ubi puncta per view (a.u.)
G
kDa
Ref(2)P
Ubi
α-Tubulin
H
Ref(2)P/α-Tubulin intensity ratio
Ubi/α-Tubulin intensity ratio
I
Control
Gak siRNA#1
Gak siRNA#2
P62
Actin
J
P62/Actin intensity ratio
Ubi/Actin intensity ratio
K
GAK siRNA#1
GAK siRNA#2
L
P62/α-Tubulin intensity ratio
M
wild type glia
GAK/daux-deficient glia
Plasma membrane
ULK1/Atg1
Atg9
Substrate
GAK/Aux
ATG13
Autophagy induction
BECLIN1
ATG14
Nucleation
Phagophore
Elongation
Autophagosome
Maturation
Lysosome
Lysosomal degradation
Autolysosome
Recycling
EE
LE
Amphisome
TGN